More Severe Hydrological Drought Events Emerge at Different Warming Levels over the Wudinghe Watershed in northern China

Yang Jiao[1,2], Xing Yuan[1,2*]

[1]School of Hydrology and Water Resources, Nanjing University of Information Science and Technology, Nanjing, 210044, Jiangsu, China

[2]Key Laboratory of Regional Climate-Environment for Temperate East Asia (RCE-TEA), Institute of Atmospheric Physics, Chinese Academy of Sciences, Beijing, 100029, China

Hydrology and Earth System Sciences

Submitted May 8, 2018

Revised December 24, 2018

[*]*Corresponding author address:* Xing Yuan, School of Hydrology and Water Resources, Nanjing University of Information Science and Technology, Nanjing, 210044, Jiangsu, China. E-mail: xyuan@nuist.edu.cn

Abstract

Assessment of changes in hydrological droughts at specific warming levels is important for an adaptive water resources management with consideration of the 2015 Paris Agreement. However, most studies focused on the response of drought frequency to the warming and neglected other drought characteristics including severity. By using a semiarid watershed in northern China (i.e., Wudinghe) as an example, here we show less frequent but more severe hydrological drought events emerge at 1.5, 2 and 3 ℃ warming levels. We used meteorological forcings from eight Coupled Model Intercomparison Project Phase 5 climate models under four representative concentration pathways, to drive a newly developed land surface hydrological model to simulate streamflow, and analyzed historical and future hydrological drought characteristics based on the Standardized Streamflow Index. The Wudinghe watershed will reach the 1.5/2/3 ℃ warming level around 2015-2034/2032-2051/2060-2079, with an increase of precipitation by 8%/9%/18% and runoff by 27%/19%/44%, and a drop of hydrological drought frequency by 11%/26%/23% as compared to the baseline period (1986-2005). However, the drought severity will rise dramatically by 184%/116%/184%, which is mainly caused by the increased variability of precipitation and evapotranspiration. The climate models and the land surface hydrological model contribute to more than 80% of total uncertainties in the future projection of precipitation and hydrological droughts. This study suggests that different aspects of hydrological droughts should be carefully investigated when assessing the impact of 1.5, 2 and 3 ℃ global warming.

Key Words: hydrological drought; 1.5, 2 and 3 ℃ warming levels; CMIP5 models; RCP scenarios; uncertainty analysis.

1. Introduction

Global warming has affected both natural and artificial systems across continents, bringing a lot of eco-hydrological crises to many countries (Gitay et al., 2002; Tirado et al., 2010; Thornton et al., 2014). The Intergovernmental Panel on Climate Change (IPCC) Fifth Assessment Report (AR5) concluded that global average surface air temperature increased by 0.61°C in 1986-2005 compared to pre-industrial periods (IPCC, 2014a). In order to mitigate global warming, the Conference of the Parties of the United Nations Framework Convention on Climate Change (UNFCCC) emphasized in the Paris Agreement that the increase in global average temperature should be controlled within 2 ℃ above preindustrial levels, and further efforts should be made to limit it below 1.5 ℃. However, whether the temperature controlling goal can be reached is still unknown, with much difficulty under current emission conditions (Peters et al., 2012). In addition, specific warming level such as 2 ℃ increase would be too high for many regions and countries (James et al., 2017; Rogelj et al., 2015). Therefore, it is necessary to assess changes in regional hydrological cycle and extremes under 1.5, 2 and even 3 ℃ global warming.

Global warming is mainly caused by greenhouse gases emissions and has a profound influence on hydrosphere and ecosphere (Barnett et al., 2005; Vorosmarty et al., 2000). It alters hydrological cycle both directly (e.g., influences precipitation and evapotranspiration) and indirectly (e.g., influences plant growth and related hydrological processes) at global (Zhu et al., 2016; McVicar et al., 2012) and local scales (Tang et al., 2013; Zheng et al., 2009; Zhang et al., 2008). Besides affecting the

mean states of the hydrological conditions, global warming also intensifies hydrological extremes significantly, such as droughts which were regarded as naturally occurring events when water (precipitation, or streamflow, etc.) is significantly below normal over a period of time (Van Loon et al., 2016; Dai, 2011). Among different types of droughts, hydrological droughts focus on the decrease in the availability of water resources, e.g., surface and/or ground water (Lorenzo-Lacruz et al., 2013). Many researchers paid attention to the historical changes, future evolutions and uncertainties, and causing factors for hydrological droughts (Chang et al., 2016; Kormos et al., 2016; Orlowsky and Seneviratne, 2013; Parajka et al., 2016; Perez et al., 2011; Prudhomme et al., 2014; Van Loon and Laaha, 2015; Wanders and Wada, 2015; Yuan et al., 2017). Most drought projection studies focused on the future changes over a fixed time period (e.g., late 21st century), but recent studies pointed out the importance on hydrological drought evolution at certain warming levels (Roudier et al., 2016; Marx et al., 2018) given the aim of the Paris Agreement. Moreover, the changes in characteristics (e.g., frequency, duration, severity) of hydrological drought events at specific warming levels received less attention. The projection of these drought characteristics could provide more relevant guidelines for policymakers on implementing adaptation strategies.

In the past five decades, a significant decrease in channel discharge was observed in the middle reaches of the Yellow River basin over northern China (Yuan et al., 2018; Zhao et al., 2014), leading to an intensified water resources scarcity in this populated area. In this study, we take a semiarid watershed, the Wudinghe in the middle reaches

of the Yellow River basin as a testbed, aiming at solving the following questions: (1) How do hydrological drought characteristics change at different warming levels over the Wudinghe watershed? (2) What are the causes for the hydrological drought change? (3) What are the contributions of uncertainties from different sources (e.g., climate and land surface hydrological models, representative concentration pathways (RCPs) scenarios, and internal variability)?

2. Study area and dataset

In this study, the Wudinghe watershed was chosen for hydrological drought analysis. As one of the largest sub-basins of the Yellow River basin, the Wudinghe watershed is located in the Loess Plateau, and has a drainage area of 30261 km^2 with Baijiachuan hydrological station as the watershed outlet (Figure 1). It has a semiarid climate with long-term (1956-2010) annual mean precipitation of 356 mm and runoff of 39 mm, resulting in a runoff coefficient of 0.11 (Jiao et al., 2017). Most of the rainfall events are concentrated in summer (June to September) with a large possibility of heavy rains (Mo et al., 2009). Located in the transition zone between cropland/grassland and desert/shrub, the northwest part of the Wudinghe watershed is dominated by sandy soil, while the major soil type for the southeast part is loess soil. During recent decades, the Wudinghe watershed has experienced a significant streamflow decrease (Yuan et al., 2018; Zhao et al., 2014) and suffered from serious water resource scarcity because of climate change, vegetation degradation and human water consumption (Xiao, 2014; Xu, 2011).

<Figure 1 here>

106 The Coupled Model Intercomparison Project Phase 5 (CMIP5) general circulation
107 model (GCM) simulations for historical experiments and future projections formed
108 the science basis for the IPCC AR5 reports (IPCC, 2014b; Taylor et al., 2012). In this
109 study, we chose eight CMIP5 GCMs for historical (1961-2005) and future (2006-2099)
110 drought analysis, as they provided daily simulations under all four RCP scenarios (i.e.
111 RCP2.6/4.5/6.0/8.5). Table 1 listed the details of GCMs used in this paper. Because of
112 the deficiency in GCM precipitation and runoff simulations, we used the corrected
113 meteorological forcing data from CMIP5 climate models, to drive a high resolution
114 land surface hydrological model to simulate runoff and streamflow.
115 <Table 1 here>
116 All CMIP5 simulations were bias corrected before being used as land surface model
117 input. After interpolating CMIP5 simulations and China Meteorological
118 Administration (CMA) station observations to the same resolution (0.01 degree in this
119 study), a modified correction method (Li et al., 2010) based on widely-used quantile
120 mapping (Wood et al., 2002; Yuan et al., 2015) was applied to adjust CMIP5/ALL
121 historical simulations and CMIP5/RCPs future simulations for each model at each
122 grid cell separately. The bias-corrected daily precipitation and temperature were then
123 further temporally disaggregated to a 6-hours interval based on the diurnal cycle
124 information from CRUNCEP 6-hourly dataset
125 (https://svn-ccsm-inputdata.cgd.ucar.edu/trunk/inputdata/atm/datm7/). Other 6-hourly
126 meteorological forcings, i.e., incident solar radiation, air pressure, specific humidity
127 and wind speed, were directly taken from CRUNCEP dataset. Please see Appendix

Section for details.

3. Land Surface Hydrological Model and Methods

3.1. Introduction of the CLM-GBHM model

In this study, we chose a newly developed land surface hydrological model, CLM-GBHM, to simulate historical and future streamflow. This model was first developed and applied in the Wudinghe watershed at 0.01 degree (Jiao et al., 2017) and then the Yellow River basin at 0.05 degree resolution (Sheng et al., 2017). By improving surface runoff generation, subsurface runoff scheme, river network-based representation and 1-D kinematic wave river routing processes, CLM-GBHM showed good performances in simulating streamflow, soil moisture content and water table depth (Sheng et al., 2017). Figure 2 demonstrated the structure and main eco-hydrological processes of CLM-GBHM. Model resolution, surface datasets, initial conditions and model parameters were kept consistent with Jiao et al. (2017), except that monthly LAI in 1982 was used for all simulations because of an unknown vegetation condition in the future.

<Figure 2 here>

3.2. Determination of years reaching specific warming levels

IPCC AR5 (IPCC, 2014a) reported that global average surface air temperature change between pre-industrial period (1850-1900) and reference period (1986-2005) is 0.61 (0.55 to 0.67) °C. Therefore, we took 1986-2005 as the baseline period. Monthly standardized streamflow index (SSI) simulations from CLM-GBHM were compared with the observed records during the baseline period, and the model performed well

150 with a correlative coefficient of 0.53 ($p<0.01$). Here, "1.5 ℃ warming level" referred
151 to a global temperature increase of 0.89 (=1.5-0.61) ℃, "2 ℃ warming level" referred
152 to an increase of 1.39 (=2-0.61) ℃, and "3 ℃ warming level" referred to an increase
153 of 2.39 (=3-0.61) ℃ compared with the baseline, respectively. As large differences
154 existed in temperature simulations among CMIP5 models and RCP scenarios, we
155 applied a widely used time sampling method (James et al., 2017; Mohammed et al.,
156 2017; Marx et al., 2018) to each GCM under each RCP scenario (referred to as
157 GCM/RCP combination hereafter). A 20-years moving window, which has the same
158 length of the baseline period, was used to determine the first period reaching a
159 specific warming level for each combination, with the period median year referred to
160 as the "crossing year".

161 **3.3. Identification of hydrological drought characteristics**

162 We used a two-step method similar to previous studies (Lorenzo-Lacruz et al., 2013;
163 Ma et al., 2015; Yuan et al., 2017) to extract hydrological drought characteristics in
164 this paper. At the first step, a hydrological drought index named as Standardized
165 Streamflow Index (SSI) was calculated by fitting monthly streamflow using a
166 probabilistic distribution function (Vicente-Serrano et al., 2012; Yuan et al., 2017).
167 Specifically, for each calendar month, streamflow values in that month during
168 baseline period were collected, arranged, and fitted by using a gamma distribution
169 function. Using the same parameters of the fitted gamma distribution, both baseline
170 (1986-2005) and future (2006-2099) streamflow values in that calendar month were
171 standardized to get SSI values. The procedure was repeated for twelve calendar

172 months, four RCP scenarios and eight GCMs separately. The second step was
173 identification and characterization of hydrological drought events by an SSI threshold
174 method (Yuan and Wood, 2013; Lorenzo-Lacruz et al., 2013; Van Loon and Laaha,
175 2015). Here, a threshold of -0.8 was selected, which is equivalent to a dry condition
176 with a probability of 20%. Months with SSI below -0.8 were treated as dry months,
177 and 3 or more continuous dry months were considered as the emergence of a
178 hydrological drought event. To characterize the hydrological drought event, drought
179 duration (months) and severity (sum of the difference between -0.8 and SSI) for a
180 certain drought event were calculated. As future SSI values were all calculated based
181 on historical values, it is important to mention that drought analysis here represented
182 those without adaptation (Samaniego et al., 2018).

183 **3.4. Uncertainty separation**

184 Given large spreads among future projections (including combinations of eight GCMs
185 and four RCP scenarios, as shown in shaded areas in Figure 3), a separation method
186 (Hawkins and Sutton, 2009; Orlowsky and Seneviratne, 2013) was applied to explore
187 uncertainty from three individual sources, i.e., internal variability, climate models and
188 RCPs scenarios. In order to separate internal variability from other two factors with
189 long-term trends, a 4^{th} order polynomial was selected to fit specific time series: the
190 fitting was first carried out during baseline period (1986-2005) to obtain an average i_m
191 as a reference value, and then during future period (2006-2099) to obtain a smooth fit
192 $x_{m,s,t}$. Future projections ($X_{m,s,t}$) were then separated into three parts: reference value
193 (i_m), smooth fit ($x_{m,s,t}$) and residual ($e_{m,s,t}$), and the uncertainties from three sources

were then calculated as follows:

$$V = \sum_{m} \mathrm{var}_{s,t}(e_{m,s,t}) / N_m \quad (1)$$

$$M_t = \sum_{s} \mathrm{var}_{m}(x_{m,s,t}) / N_s \quad (2)$$

$$S_t = \mathrm{var}_{s}(\sum_{m} x_{m,s,t} / N_m) \quad (3)$$

where V, M_t and S_t represent uncertainties from internal variability (which is time-invariant), climate models and RCPs scenarios, N_m and N_s are numbers of climate models and RCPs scenarios, $\mathrm{var}_{s,t}$ denotes the variance across scenarios and time, var_m and var_s are variances across models and scenarios respectively. Finally, uncertainty contributions from each component were calculated as proportions to the sum. In this study, we applied this method to the 20-years moving averaged ensemble time series.

4. Results

4.1. Changes in hydrometeorology in the past and future

We first calculated the trends during both the historical and future periods for basin-averaged annual mean hydrological variables (Table 2 and Figure 3). During 1961-2005, there was a significant increasing trend ($p<0.01$) in observed temperature and a decreasing trend ($p<0.1$) in observed precipitation, resulted in a decreasing naturalized streamflow ($p<0.01$) and an increasing hydrological drought frequency ($p<0.01$). Here, the naturalized streamflow was obtained by adding human water use back to the observed streamflow (Yuan et al., 2017). These historical changes could be captured by hydro-climate model simulations to some extent, although both the warming and drying trends were underestimated (Table 2). Ensemble monthly SSI

213 series from GCM driven model simulations were also compared with offline results
214 (CRUNCEP driven) during historical period, resulted in a correlative coefficient of
215 0.47 ($p<0.01$). During 2006-2099, four variables show consistent changing trends
216 across RCPs scenarios, but with different magnitudes (Table 2). Future temperature
217 and precipitation will increase, resulting in an increasing streamflow and decreasing
218 hydrological drought frequency. Unlike temperature trends that increase from RCP2.6
219 to RCP8.5 (which indicates different radiative forcings), precipitation trend under
220 RCP6.0 is smaller than that under RCP4.5, suggesting a nonlinear response of
221 regional water cycle to the increase in radiative forcings. As a result, RCP6.0 shows
222 the smallest increasing rate in streamflow and decreasing rate in drought frequency.
223 <Table 2 here>
224 More details could be found in Figure 3 when focusing on dynamic changes in the
225 history and future. Figure 3a shows that the differences in temperature among RCPs
226 are negligible until 2030s when RCP8.5 starts to outclass other scenarios, and the
227 others begin to diverge in the far future (2060s-2080s). In contrast, differences in
228 future precipitation are small throughout the 21st century, except that RCP8.5 scenario
229 becomes larger after 2080s (Figure 3b). As comprehensive outcomes of climate and
230 eco-hydrological factors, a clear decrease-increase pattern in streamflow and an
231 increase-decrease trend in hydrological drought frequency are found (Figure 3c and
232 3d). However, differences among RCPs are not discernible. Figures 3b-3d also show
233 that the differences in water-related variables among climate models are very large.
234 <Figure 3 here>

235 Using the time-sampling method mentioned in Section 3.2, first 20-year periods with
236 mean temperature increasing across 1.5, 2 and 3 ℃ warming levels for each
237 GCM/RCP combination were identified and listed in Table 3. To demonstrate the
238 overall situation for a specific warming level, we chose median year among GCMs as
239 model ensemble for each RCP scenario, and median year among all GCMs and RCPs
240 as total ensemble. GCM/RCP combinations not reaching specific warming level were
241 marked as "NR" in Table 3 and were not considered when calculating ensemble year.
242 <Table 3 here>
243 As listed in Table 3, crossing years for most GCM/RCP combinations reaching 1.5 ℃
244 warming level are before 2032 except for GFDL-ESM2M and MRI-CGCM3. Model
245 ensemble years for different RCP scenarios have small differences, and total ensemble
246 year for all GCMs and RCPs is 2025, indicating that 1.5 ℃ warming level would be
247 reached within 2015-2034. As for 2 and 3 ℃ warming level, the total ensemble year is
248 2042 and 2070, respectively. There are large differences in crossing years among
249 different GCMs, ranging from 2016 to 2075 for 1.5 ℃, 2030 to 2076 for 2 ℃, and
250 2051 to 2086 for 3 ℃. Generally, three global warming thresholds would be reached
251 first under RCP8.5 and last under RCP6.0 scenario. All GCMs will not reach 3 ℃
252 warming level under RCP2.6, while under other RCP scenarios this temperature
253 increase would probably be reached around 2073 or even as early as 2050s.
254 **4.2. Hydrological changes at 1.5, 2 and 3 ℃ warming levels**
255 After identifying the time periods reaching specific warming levels, we collected
256 precipitation and runoff data within these periods (different among GCM/RCP

257 combinations), and calculated their relative changes compared to the baseline period
258 (1986-2005). Figure 4 shows the spatial pattern of relative changes in model ensemble
259 mean precipitation of these time periods, except for the period under RCP2.6 at 3 ℃
260 warming level during which no sample exists. Results indicate that precipitation will
261 increase at all warming levels and all RCP scenarios, while differences exist in spatial
262 patterns. The ensemble mean precipitation increases by 8.0%, 9.1% and 18.0% at 1.5,
263 2 and 3 ℃ warming levels for all RCP scenarios respectively, indicating larger
264 increase in precipitation when warming level increases. For each warming level,
265 precipitation changes among all RCP scenarios are quite close except for RCP6.0 at
266 3 ℃ warming level. Larger precipitation increases generally occur in the south and
267 southwest parts which are upstream regions of the Wudinghe watershed.
268 <Figure 4 here>
269 The watershed-mean runoff increases by 26.7%, 18.7% and 44.5% at each warming
270 level respectively, which are larger than those of precipitation because of nonlinear
271 hydrological response (Figure 5). For all warming levels, RCP8.5 shows greatest
272 runoff increase and RCP2.6/6.0 the lowest. Small or negative changes in runoff
273 emerge in the north and southeast regions under RCP2.6/4.5/6.0 scenarios (Figure 5),
274 where precipitation increases the least (Figure 4). Besides, runoff changes are also
275 closely linked to watershed river networks, with large increase in the south and
276 middle parts (upper and middle reaches) and small increase or even decrease in the
277 southeast and northeast parts (lower reaches), showing the redistribution effect of
278 surface topography and soil property.

279 <Figure 5 here>

280 Figure 6 shows the characteristics of hydrological droughts during baseline period and
281 the periods reaching all warming levels. The number of hydrological drought events
282 averaged among all RCP scenarios and climate models is 7 in the baseline period, and
283 it drops to 6.2 (-11% relative to baseline, the same below) at 1.5 ℃, 5.2 (-26%) at
284 2 ℃ and 5.4 (-23%) at 3 ℃ warming levels (Figure 6a). However, hydrological
285 drought duration increases from 5 months at baseline to 6.5 (+30%), 5.9 (+18%) and 6
286 months (+20%) at 1.5, 2 and 3 ℃ warming levels, respectively. Drought severity
287 increases dramatically from 1.9 at baseline to 5.4 (+184%) at 1.5 ℃ warming level,
288 and then drops to 4.1 (+116%) at 2 ℃ warming level and rebounds to 5.4 (+184%) at
289 3 ℃ warming level (Figure 6a). These results indicate that although precipitation and
290 runoff increase, the Wudinghe watershed would suffer from more severe hydrological
291 events in the near future at 1.5 ℃ warming level. The severity could be alleviated in
292 time periods reaching 2 ℃ warming level, with more precipitation occurring over the
293 watershed.

294 <Figure 6 here>

295 The analysis on individual scenarios suggests a similar conclusion (Figures 6b-6e).
296 Drought amount and severity increase generally when radiative forcing increases. The
297 least changes in drought severity are found under RCP4.5 scenario while the largest
298 changes are under RCP6.0 scenario. Higher warming levels could lead to more
299 moderate drought events under low emission scenarios (RCP2.6/4.5) because of more
300 precipitation in the near future, while high emissions (RCP6.0/8.5) would increase the

301 risk of hydrological drought significantly.

302 **5. Discussion**

303 To explore the reason for less frequent but more severe hydrological droughts, we
304 compared the differences in monthly precipitation, evapotranspiration,
305 total/surface/sub-surface runoff and streamflow between the baseline period and
306 periods reaching 1.5, 2 and 3 ℃ warming levels. Standardized indices for these
307 hydrological variables were used to remove seasonality from monthly time series, and
308 mean values and variabilities of these indices were chosen as indicators.

309 <Figure 7 here>

310 Figure 7 shows that mean values increase as temperature increases for all standardized
311 hydrological indices, showing a wetter hydroclimate in the future with more
312 precipitation, evapotranspiration, runoff and streamflow (Figure 7a). However,
313 variabilities for the standardized indices in the future are much higher than those
314 during baseline period, indicating larger fluctuations and higher chance for extreme
315 droughts/floods at all warming levels (Figure 7b). For extreme drought events (with
316 an SSI < -1.3, representing a dry condition with a probability of 10%), the ensemble
317 mean amount of drought events are 4.3, 3.1 and 3.7 at 1.5, 2 and 3 ℃ warming levels,
318 which are much larger than the baseline period with 0.9 (not shown). Focusing on the
319 gaps between baseline and future periods, it is clear that the differences in both
320 evapotranspiration and runoff are larger than those of precipitation for mean values
321 and standard deviations, suggesting the water redistribution through complicated
322 hydrological processes. The increase in mean value of runoff and consequently

streamflow mainly comes from the increase in subsurface runoff. As hydrological drought defined in this paper is based on monthly SSI series, increases in both mean value and variability in precipitation and evapotranspiration indicate a period with less frequent but more severe hydrological drought events.

Another issue is the reliability of results considering large differences among CMIP5 models. Figure 8 shows the uncertainty fractions contributed from internal variability, climate models and RCPs scenarios based on multi-model and multi-scenario ensemble projections of temperature, precipitation, streamflow and drought frequency. Uncertainty in temperature projection is mainly contributed by climate models before 2052, and it is then taken over by RCPs scenarios. Internal variability contributes to less than 1.5% of the uncertainty for the temperature projection (Figure 8a). For precipitation projection, climate models account for a large proportion of uncertainty throughout the century. The internal variability contributes to larger uncertainty than RCPs scenarios until the second half of the 21st century (Figure 8b). Similar to precipitation, major source of uncertainty for the projections of streamflow and hydrological drought frequency comes from climate and land surface hydrological models, while the impacts of both internal variability and RCP scenarios are further weakened (Figures 8c-8d).

<Figure 8 here>

Generally for all variables except temperature, GCMs and land surface hydrological model account for over 80% of total uncertainties, while internal variability contributes to a comparable or larger proportion than RCPs scenarios. RCPs scenario

only contributes to around 5% of the uncertainties in the projections of streamflow and hydrological drought frequency. These results indicate that the improvement in GCM simulated precipitation would largely narrow the uncertainties for future projections of hydrological droughts. Besides, previous studies (Marx et al., 2018; Samaniego et al., 2018) have shown that uncertainties contributed from land surface hydrological models can be comparable to that from GCMs, indicating the importance of introducing multiple land surface hydrological models into the analysis of uncertainty, and the significance of exploring more suitable methods in further studies.

There are also some issues for further investigations. As shown in Figure 3, GCM historical simulations underestimates the increasing trend in temperature and decreasing trend in precipitation, and results in underestimations of hydrological drying trends. Although the quantile mapping method used in this study is able to remove the biases in GCM simulations (e.g., mean value, variance), the underestimation of trends could not be corrected. An alternative method is to use regional climate models for dynamical downscaling, which would be useful if regional forcings (e.g., topography, land use change, aerosol emission) are strong. Another issue is about the spatially varied warming rates. IPCC AR5 reported (IPCC, 2014c) that global warming for the last 20 years compared to pre-industrial are 0.3-1.7 ℃ (RCP2.6), 1.1-2.6 ℃ (RCP4.5), 1.4-3.1 ℃ (RCP6.0), 2.6-4.8 ℃ (RCP8.5). However, temperature increases vary a lot for different regions. For instance, temperature rises faster in high-altitude (Kraaijenbrink et al., 2017) and polar regions

(Bromwich et al., 2013), where the rate of regional warming could be three times of global warming. Actually, reaching periods for regional warming thresholds in the Wudinghe watershed are earlier than the global ones (not shown here), which suggest that the regional warming would be more severe at specific global warming levels.

6. Conclusions

In this paper, we bias-corrected future projections of meteorological forcings from eight CMIP5 GCM simulations under four RCP scenarios to drive a newly developed land surface hydrological model, CLM-GBHM, to project changes in streamflow and hydrological drought characteristics over the Wudinghe watershed. After determining the time periods reaching 1.5, 2 and 3 ℃ global warming levels for each GCM/RCP combination, we focused on the changes in regional hydrological drought characteristics at all warming levels. Moreover, projection uncertainties from different sources were separated and analyzed. Main conclusions are listed as follows:

(1) With CMIP5 GCM simulations as forcing data, the model ensemble mean hindcast can reproduce the significant decreasing trend of streamflow and increasing trend of hydrological drought frequency in historical period (1961-2005), but the drying trend is underestimated because of GCM uncertainties. Streamflow increases and hydrological drought frequency decreases in the future under all RCP scenarios.

(2) The time periods reaching 1.5, 2 and 3 ℃ warming levels over the Wudinghe watershed are 2015-2034, 2032-2051 and 2060-2079, respectively. There are large differences in results among different GCMs, while different RCP scenarios show consistence in reaching periods with RCP8.5 the earliest and RCP6.0 the latest.

(3) Precipitation increases under all RCP scenarios at all warming levels (8%, 9% and 18%), while differences exist in spatial patterns. Runoff has larger relative change rates (27%, 19% and 44%), with larger increases of runoff occurred in the upper and middle reaches and less increases or even decreases emerged in the lower reaches, indicating a complex spatial distribution in hydrological droughts.

(4) As a result of increasing mean values and variability for precipitation, evapotranspiration and runoff, hydrological drought frequency drops by 11%-26% at all warming levels compared to the baseline period, while hydrological drought severity rises dramatically by 116%-184%. This indicates that the Wudinghe watershed would suffer more severe hydrological drought events in the future, especially under RCP6.0 and RCP8.5 scenarios.

(5) The main uncertainty sources vary among hydrological variables. Most uncertainties are from climate and land surface models, especially for precipitation. At all warming levels, models contribute to over 80% of total uncertainties, while internal variability contributes to a comparable proportion of uncertainties to RCPs scenarios for precipitation, streamflow and hydrological drought frequency.

Acknowledgements

We would like to thank the editor and two anonymous reviewers for their helpful comments. This research was supported by National Key R&D Program of China (2018YFA0606002), Strategic Priority Research Program of Chinese Academy of Sciences (XDA20020201), National Natural Science Foundation of China (91547103),

and the Startup Foundation for Introducing Talent of NUIST. Daily precipitation and temperature simulated by CMIP5 models were provided by the World Climate Research Programme's Working Group on Coupled Modeling (https://esgf-data.dkrz.de/search/cmip5-dkrz). We thank Prof. Dawen Yang and Prof. Huimin Lei for the implementation of the CLM-GBHM land surface hydrological model.

Appendix: Details of Processing Climate Forcings

The land surface hydrological model CLM-GBHM requires a list of input climate forcings, i.e. precipitation, near surface air temperature, incident solar radiation, air pressure, specific humidity and wind speed. These variables were generated from three datasets in this study: CMIP5 daily simulations during both historical (1961-2005) and future (2006-2099) periods, CRUNCEP 6-hourly dataset during 1959-2005, and China Meteorological Administration (CMA) daily station observations during 1961-2005. All datasets were firstly regridded to the same resolution (0.01 degree) by using bilinear interpolation method for further processing. After spatial interpolation, daily precipitation and temperature from CMIP5 simulations were adjusted to remove their monthly biases compared to CMA observations, by applying a correction method to each model at each grid cell separately. This method modified the widely used quantile-mapping method (CDFm) and processed historical and future timeseries in different ways. For historical period, bias-corrected monthly variable x (i.e., precipitation or temperature) was calculated

433 based on CDFm:

$$x_{sim,his,corrected} = F^{-1}_{obs,his}(F_{sim,his}(x_{sim,his,biased})) \quad \text{(A1)}$$

434 where F is cumulative distribution function of variable x, subscripts *sim*, *obs*, *his*,
435 *biased*, *corrected* represent simulated value, observed value, historical period, value
436 with bias and value after bias correction at monthly scale, respectively. The basic
437 assumption of CDFm is that the climate distribution does not change much over time,
438 however, this is invalid considering intense global warming in the future. Therefore,
439 an equidistant CDF matching method (EDCDFm; Li et al., 2010) was applied for
440 future projections, which assumes that the difference between simulated and observed
441 values remains the same over time:

$$\begin{aligned} &x_{sim,fut,corrected} = \\ &x_{sim,fut,biased} + F^{-1}_{obs,his}(F_{sim,fut}(x_{sim,fut,biased})) - F^{-1}_{sim,his}(F_{sim,fut}(x_{sim,fut,biased})) \end{aligned} \quad \text{(A2)}$$

442 where subscript *fut* represents future period. After bias correction at monthly scale,
443 new daily precipitation (temperature) series were generated based on the ratio
444 (difference) between the new and old CMIP5 simulated monthly means:

$$P_{d,corrected} = (P_{m,corrected} / P_{m,biased}) \cdot P_{d,biased} \quad \text{(A3)}$$

$$T_{d,corrected} = (T_{m,corrected} - T_{m,biased}) + T_{d,biased} \quad \text{(A4)}$$

445 where P and T represent precipitation and temperature, subscripts d and m represent
446 daily value and corresponding monthly mean, respectively.

447 In order to temporally disaggregate daily temperature and precipitation to a 6-hours
448 interval during both historical and future periods, the diurnal cycle information from
449 CRUNCEP dataset was introduced. By looping the CRUNCEP data during 1959-2005
450 (47 years) twice, we could also generate "future data" (2006-2099, 94 years). By

451 using the same disaggregation method that downscales variables from monthly to
452 daily, temporal downscaling from daily to 6-hourly scales was achieved:

$$P_{6h,corrected} = (P_{d,corrected} / P_{d,CRUNCEP}) \cdot P_{6h,CRUNCEP} \quad \text{(A5)}$$

$$T_{6h,corrected} = (T_{d,corrected} - T_{d,CRUNCEP}) + T_{6h,CRUNCEP} \quad \text{(A6)}$$

453 where subscript *6h* represents 6-hourly values. It should be mentioned that only
454 precipitation and temperature have been used from CMIP5 models, with other climate
455 forcing variables (i.e., incident solar radiation, air pressure, specific humidity and
456 wind speed series) directly taken from CRUNCEP dataset. Whether physical
457 consistency among all climate forcing variables was maintained or not by simply
458 introducing CRUNCEP dataset was not considered in this study, and it is unclear how
459 the climate change signals by GCMs might be affected by using CRUNCEP data for a
460 majority of forcing variables. Although resampling methods (e.g., Schaake Shuffle)
461 that are widely used in temporal downscaling for seasonal forecasting might result in
462 more consistent forcing variables, whether such consistency (e.g.,
463 temperature-humidity relationship) holds for future projection given the changing
464 climate is unknown. More sophisticated downscaling techniques (either statistical or
465 dynamical) are needed for further studies.
466
467

References

Barnett, T. P., Adam, J. C., and Lettenmaier, D. P.: Potential impacts of a warming climate on water availability in snow-dominated regions, Nature, 438, 303-309, doi:10.1038/nature04141, 2005.

Bromwich, D. H., Nicolas, J. P., Monaghan, A. J., Lazzara, M. A., Keller, L. M., Weidner, G. A., and Wilson, A. B.: Central West Antarctica among the most rapidly warming regions on Earth, Nat Geosci, 6, 139-145, doi:10.1038/Ngeo1671, 2013.

Chang, J., Li, Y., Wang, Y., and Yuan, M.: Copula-based drought risk assessment combined with an integrated index in the Wei River Basin, China, Journal of Hydrology, 540, 824-834, doi:10.1016/j.jhydrol.2016.06.064, 2016.

Dai, A. G.: Drought under global warming: a review, Wires Clim Change, 2, 45-65, doi:10.1002/wcc.81, 2011.

Gitay, H., Suárez, A., Watson, R. T., and Dokken, D. J.: Climate change and biodiversity, IPCC Technical Paper V, 2002.

Hawkins, E., and Sutton, R.: The Potential to Narrow Uncertainty in Regional Climate Predictions, B Am Meteorol Soc, 90, 1095-+, doi:10.1175/2009bams2607.1, 2009.

IPCC: Climate Change 2013 - The Physical Science Basis, Cambridge University Press, Cambridge, United Kingdom and New York, NY, USA, 1535 pp., 2014a.

IPCC: Summary for Policymakers, in: Climate Change 2013 - The Physical Science Basis, edited by: Stocker, T. F., Qin, D., Plattner, G.-K., Tignor, M., Allen, S. K., Boschung, J., Nauels, A., Xia, Y., Bex, V., and Midgley, P. M., Cambridge University Press, Cambridge, United Kingdom and New York, NY, USA, 1-30, 2014b.

IPCC: Long-term Climate Change: Projections, Commitments and Irreversibility, in: Climate Change 2013 - The Physical Science Basis, edited by: Stocker, T. F., Qin, D., Plattner, G.-K., Tignor, M., Allen, S. K., Boschung, J., Nauels, A., Xia, Y., Bex, V., and Midgley, P. M., Cambridge University Press, Cambridge,

United Kingdom and New York, NY, USA, 1029-1136, 2014c.

James, R., Washington, R., Schleussner, C. F., Rogelj, J., and Conway, D.: Characterizing half-a-degree difference: a review of methods for identifying regional climate responses to global warming targets, Wires Clim Change, 8, doi:10.1002/wcc.457, 2017.

Jiao, Y., Lei, H. M., Yang, D. W., Huang, M. Y., Liu, D. F., and Yuan, X.: Impact of vegetation dynamics on hydrological processes in a semi-arid basin by using a land surface-hydrology coupled model, Journal of Hydrology, 551, 116-131, doi:10.1016/j.jhydrol.2017.05.060, 2017.

Kormos, P. R., Luce, C. H., Wenger, S. J., and Berghuijs, W. R.: Trends and sensitivities of low streamflow extremes to discharge timing and magnitude in Pacific Northwest mountain streams, Water Resour Res, 52, 4990-5007, doi:10.1002/2015wr018125, 2016.

Kraaijenbrink, P. D. A., Bierkens, M. F. P., Lutz, A. F., and Immerzeel, W. W.: Impact of a global temperature rise of 1.5 degrees Celsius on Asia's glaciers, Nature, 549, 257-+, doi:10.1038/nature23878, 2017.

Li, H. B., Sheffield, J., and Wood, E. F.: Bias correction of monthly precipitation and temperature fields from Intergovernmental Panel on Climate Change AR4 models using equidistant quantile matching, J Geophys Res-Atmos, 115, doi:10.1029/2009jd012882, 2010.

Lorenzo-Lacruz, J., Moran-Tejeda, E., Vicente-Serrano, S. M., and Lopez-Moreno, J. I.: Streamflow droughts in the Iberian Peninsula between 1945 and 2005: spatial and temporal patterns, Hydrology and Earth System Sciences, 17, 119-134, doi:10.5194/hess-17-119-2013, 2013.

Ma, F., Yuan, X., and Ye, A. Z.: Seasonal drought predictability and forecast skill over China, J Geophys Res-Atmos, 120, 8264-8275, doi:10.1002/2015jd023185, 2015.

Marx, A., Kumar, R., Thober, S., Rakovec, O., Wanders, N., Zink, M., Wood, E. F., Pan, M., Sheffield, J., and Samaniego, L.: Climate change alters low flows in Europe under global warming of 1.5, 2, and 3 degrees C, Hydrology and Earth

System Sciences, 22, 1017-1032, doi:10.5194/hess-22-1017-2018, 2018.

McVicar, T. R., Roderick, M. L., Donohue, R. J., Li, L. T., Van Niel, T. G., Thomas, A., Grieser, J., Jhajharia, D., Himri, Y., Mahowald, N. M., Mescherskaya, A. V., Kruger, A. C., Rehman, S., and Dinpashoh, Y.: Global review and synthesis of trends in observed terrestrial near-surface wind speeds: Implications for evaporation, Journal of Hydrology, 416, 182-205, doi:10.1016/j.jhydrol.2011.10.024, 2012.

Mo, X. G., Liu, S. X., Chen, D., Lin, Z. H., Guo, R. P., and Wang, K.: Grid-size effects on estimation of evapotranspiration and gross primary production over a large Loess Plateau basin, China, Hydrolog Sci J, 54, 160-173, doi:10.1623/hysj.54.1.160, 2009.

Mohammed, K., Islam, A. S., Islam, G. M. T., Alfieri, L., Bala, S. K., and Khan, M. J. U.: Extreme flows and water availability of the Brahmaputra River under 1.5 and 2 A degrees C global warming scenarios, Climatic Change, 145, 159-175, doi:10.1007/s10584-017-2073-2, 2017.

Orlowsky, B., and Seneviratne, S. I.: Elusive drought: uncertainty in observed trends and short- and long-term CMIP5 projections, Hydrology and Earth System Sciences, 17, 1765-1781, doi:10.5194/hess-17-1765-2013, 2013.

Parajka, J., Blaschke, A. P., Bloeschl, G., Haslinger, K., Hepp, G., Laaha, G., Schoener, W., Trautvetter, H., Viglione, A., and Zessner, M.: Uncertainty contributions to low-flow projections in Austria, Hydrology and Earth System Sciences, 20, 2085-2101, doi:10.5194/hess-20-2085-2016, 2016.

Perez, G. A. C., van Huijgevoort, M. H. J., Voss, F., and van Lanen, H. A. J.: On the spatio-temporal analysis of hydrological droughts from global hydrological models, Hydrology and Earth System Sciences, 15, 2963-2978, doi:10.5194/hess-15-2963-2011, 2011.

Peters, G. P., Andrew, R. M., Boden, T., Canadell, J. G., Ciais, P., Le Quéré, C., Marland, G., Raupach, M. R., and Wilson, C.: The challenge to keep global warming below 2 C, Nat Clim Change, 3, 4, 2012.

Prudhomme, C., Giuntoli, I., Robinson, E. L., Clark, D. B., Arnell, N. W., Dankers,

557 R., Fekete, B. M., Franssen, W., Gerten, D., Gosling, S. N., Hagemann, S.,
558 Hannah, D. M., Kim, H., Masaki, Y., Satoh, Y., Stacke, T., Wada, Y., and
559 Wisser, D.: Hydrological droughts in the 21st century, hotspots and uncertainties
560 from a global multimodel ensemble experiment, Proceedings of the National
561 Academy of Sciences, 111, 3262-3267, doi:10.1073/pnas.1222473110, 2014.
562 Rogelj, J., Luderer, G., Pietzcker, R. C., Kriegler, E., Schaeffer, M., Krey, V., and
563 Riahi, K.: Energy system transformations for limiting end-of-century warming to
564 below 1.5 degrees C, Nat Clim Change, 5, 519-+, doi:10.1038/nclimate2572,
565 2015.
566 Roudier, P., Andersson, J. C. M., Donnelly, C., Feyen, L., Greuell, W., and Ludwig,
567 F.: Projections of future floods and hydrological droughts in Europe under a+2
568 degrees C global warming, Climatic Change, 135, 341-355,
569 doi:10.1007/s10584-015-1570-4, 2016.
570 Samaniego, L., Thober, S., Kumar, R., Wanders, N., Rakovec, O., Pan, M., Zink, M.,
571 Sheffield, J., Wood, E., and Marx, A.: Anthropogenic warming exacerbates
572 European soil moisture droughts, Nat Clim Change, 8, 421, 2018, doi:
573 10.1038/s41558-018-0138-5
574 Sheng, M. Y., Lei, H. M., Jiao, Y., and Yang, D. W.: Evaluation of the Runoff and
575 River Routing Schemes in the Community Land Model of the Yellow River
576 Basin, J Adv Model Earth Sy, 9, 2993-3018, doi:10.1002/2017ms001026, 2017.
577 Tang, Y., Tang, Q., Tian, F., Zhang, Z., and Liu, G.: Responses of natural runoff to
578 recent climatic variations in the Yellow River basin, China, Hydrology and Earth
579 System Sciences, 17, 4471-4480, doi: 10.5194/hess-17-4471-2013, 2013.
580 Taylor, K. E., Stouffer, R. J., and Meehl, G. A.: An Overview of Cmip5 and the
581 Experiment Design, B Am Meteorol Soc, 93, 485-498,
582 doi:10.1175/Bams-D-11-00094.1, 2012.
583 Thornton, P. K., Ericksen, P. J., Herrero, M., and Challinor, A. J.: Climate variability
584 and vulnerability to climate change: a review, Global Change Biol, 20,
585 3313-3328, doi:10.1111/gcb.12581, 2014.
586 Tirado, M. C., Clarke, R., Jaykus, L. A., McQuatters-Gollop, A., and Franke, J. M.:

587 Climate change and food safety: A review, Food Res Int, 43, 1745-1765,
588 doi:10.1016/j.foodres.2010.07.003, 2010.
589 Van Loon, A. F., and Laaha, G.: Hydrological drought severity explained by climate
590 and catchment characteristics, Journal of Hydrology, 526, 3-14,
591 doi:10.1016/j.jhydrol.2014.10.059, 2015.
592 Van Loon, A. F., Stahl, K., Di Baldassarre, G., Clark, J., Rangecroft, S., Wanders, N.,
593 Gleeson, T., Van Dijk, A. I. J. M., Tallaksen, L. M., Hannaford, J., Uijlenhoet, R.,
594 Teuling, A. J., Hannah, D. M., Sheffield, J., Svoboda, M., Verbeiren, B.,
595 Wagener, T., and Van Lanen, H. A. J.: Drought in a human-modified world:
596 reframing drought definitions, understanding, and analysis approaches,
597 Hydrology and Earth System Sciences, 20, 3631-3650,
598 doi:10.5194/hess-20-3631-2016, 2016.
599 Vicente-Serrano, S. M., Lopez-Moreno, J. I., Begueria, S., Lorenzo-Lacruz, J.,
600 Azorin-Molina, C., and Moran-Tejeda, E.: Accurate Computation of a
601 Streamflow Drought Index, J Hydrol Eng, 17, 318-332,
602 doi:10.1061/(Asce)He.1943-5584.0000433, 2012.
603 Vorosmarty, C. J., Green, P., Salisbury, J., and Lammers, R. B.: Global water
604 resources: Vulnerability from climate change and population growth, Science,
605 289, 284-288, doi:10.1126/science.289.5477.284, 2000.
606 Wanders, N., and Wada, Y.: Human and climate impacts on the 21st century
607 hydrological drought, Journal of Hydrology, 526, 208-220,
608 doi:10.1016/j.jhydrol.2014.10.047, 2015.
609 Wood, A. W., Maurer, E. P., Kumar, A., and Lettenmaier, D. P.: Long-range
610 experimental hydrologic forecasting for the eastern United States, J Geophys
611 Res-Atmos, 107, doi:10.1029/2001jd000659, 2002.
612 Xiao, J. F.: Satellite evidence for significant biophysical consequences of the "Grain
613 for Green" Program on the Loess Plateau in China, J Geophys Res-Biogeo, 119,
614 2261-2275, doi:10.1002/2014jg002820, 2014.
615 Xu, J. X.: Variation in annual runoff of the Wudinghe River as influenced by climate
616 change and human activity, Quatern Int, 244, 230-237,

617 doi:10.1016/j.quaint.2010.09.014, 2011.
618 Yuan, X., and Wood, E. F.: Multimodel seasonal forecasting of global drought onset,
619 Geophys Res Lett, 40, 4900-4905, doi:10.1002/grl.50949, 2013.
620 Yuan, X., Roundy, J. K., Wood, E. F., and Sheffield, J.: Seasonal forecasting of
621 global hydrologic extremes: system development and evaluation over GEWEX
622 basins, B Am Meteorol Soc, 96, 1895-1912, doi:10.1175/BAMS-D-14-00003.1,
623 2015.
624 Yuan, X., Zhang, M., Wang, L. Y., and Zhou, T.: Understanding and seasonal
625 forecasting of hydrological drought in the Anthropocene, Hydrology and Earth
626 System Sciences, 21, 5477-5492, doi:10.5194/hess-21-5477-2017, 2017.
627 Yuan, X., Y. Jiao, D. Yang, and H. Lei: Reconciling the attribution of changes in
628 streamflow extremes from a hydroclimate perspective, Water Resour Res,
629 doi:10.1029/2018WR022714, 2018
630 Zhang, X. P., Zhang, L., Zhao, J., Rustomji, P., and Hairsine, P.: Responses of
631 streamflow to changes in climate and land use/cover in the Loess Plateau, China,
632 Water Resour Res, 44, doi:10.1029/2007wr006711, 2008.
633 Zhao, G. J., Tian, P., Mu, X. M., Jiao, J. Y., Wang, F., and Gao, P.: Quantifying the
634 impact of climate variability and human activities on streamflow in the middle
635 reaches of the Yellow River basin, China, Journal of Hydrology, 519, 387-398,
636 doi:10.1016/j.jhydrol.2014.07.014, 2014.
637 Zheng, H. X., Zhang, L., Zhu, R. R., Liu, C. M., Sato, Y., and Fukushima, Y.:
638 Responses of streamflow to climate and land surface change in the headwaters of
639 the Yellow River Basin, Water Resour Res, 45, doi:10.1029/2007wr006665,
640 2009.
641 Zhu, Z. C., Piao, S. L., Myneni, R. B., Huang, M. T., Zeng, Z. Z., Canadell, J. G.,
642 Ciais, P., Sitch, S., Friedlingstein, P., Arneth, A., Cao, C. X., Cheng, L., Kato, E.,
643 Koven, C., Li, Y., Lian, X., Liu, Y. W., Liu, R. G., Mao, J. F., Pan, Y. Z., Peng,
644 S. S., Penuelas, J., Poulter, B., Pugh, T. A. M., Stocker, B. D., Viovy, N., Wang,
645 X. H., Wang, Y. P., Xiao, Z. Q., Yang, H., Zaehle, S., and Zeng, N.: Greening of
646 the Earth and its drivers, Nat Clim Change, 6, 791-795,

647 doi:10.1038/nclimate3004, 2016.

Figure Captions

Figure 1. Location, elevation and river networks for the Wudinghe watershed.

Figure 2. Structure and main eco-hydrological processes for the land surface hydrological model CLM-GBHM. (modified from Jiao et al., 2017)

Figure 3. Historical (ALL) and future (RCP2.6/4.5/6.0/8.5) time series of standardized annual mean (a) temperature, (b) precipitation and (c) streamflow, and (d) the time series of hydrological drought frequency (drought months for each year) over the Wudinghe watershed. Shaded areas indicate the ranges between maximum and minimum values among CMIP5/CLM-GBHM model simulations. ALL represents historical simulations with both anthropogenic and natural forcings, RCP2.6/4.5/6.0/8.5 represent four representative concentration pathways from lower to higher emission scenarios.

Figure 4. Spatial pattern of relative changes in multi-model ensemble mean precipitation at 1.5, 2 and 3 ℃ warming levels compared to the baseline period (1986-2005). The percentages in the upper-right corners of each panel are the watershed-mean changes for different RCP scenarios, and the percentages in the top brackets are the mean values from four RCP scenarios.

Figure 5. The same as **Figure 4**, but for the spatial patterns of runoff changes.

Figure 6. Comparison of the characteristics (amount (number of drought events per 20 years), duration (months) and severity) averaged among climate models and RCP scenarios for hydrological drought events during the baseline period (1986-2005) and the periods reaching 1.5, 2 and 3 ℃ warming levels. Black lines indicate 5%-95%

670 confidence intervals.

671 **Figure 7.** Comparison of (a) mean values and (b) standard deviations for hydrological
672 indices averaged among climate models and RCP scenarios during the baseline period
673 (1986-2005) and the periods reaching 1.5, 2 and 3 ℃ warming levels. SPI, SEI, SRI,
674 SSRI, SBI, SSI represent standardized indices of precipitation, evapotranspiration,
675 runoff, surface runoff, baseflow (subsurface runoff) and streamflow, respectively.

676 **Figure 8.** Fractions of uncertainties from internal variability (orange), RCP scenarios
677 (green) and climate and land surface hydrological models (blue) for the projections of
678 20-years moving averaged (a) temperature, (b) precipitation (c) streamflow and (d)
679 hydrological drought frequency.

680

681 **Table Captions**

682 **Table 1.** CMIP5 model simulations used in this study. ALL represents historical
683 simulations with both anthropogenic and natural forcings (r1i1p1 realization),
684 RCP2.6/4.5/6.0/8.5 represent four representative concentration pathways from lower
685 to higher emission scenarios.

686 **Table 2.** Trends in hydrometeorological variables and hydrological drought frequency
687 over the Wudinghe watershed. Historical observed trends for streamflow and drought
688 frequency were calculated by using naturalized streamflow data (Yuan et al., 2017).
689 Here, "*" and "**" indicate 90% and 99% confidence levels, respectively, while those
690 without any "*" show no significant changes ($p>0.1$).

691 **Table 3.** Determination of crossing year for the periods reaching 1.5, 2 and 3 ℃

warming levels for different GCMs and RCPs combinations. Here, “NR” means that the corresponding GCM/RCP combination will not reach the specified warming level throughout the 21st century.

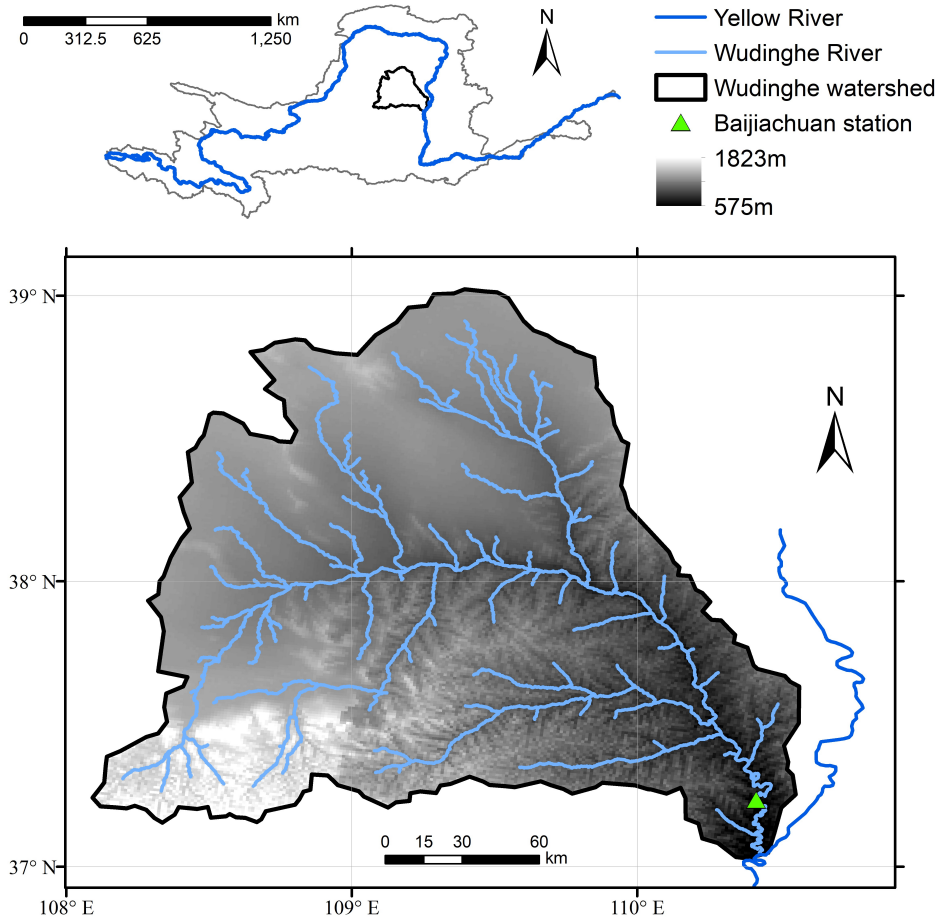

696

697 **Figure 1.** Location, elevation and river networks for the Wudinghe watershed.

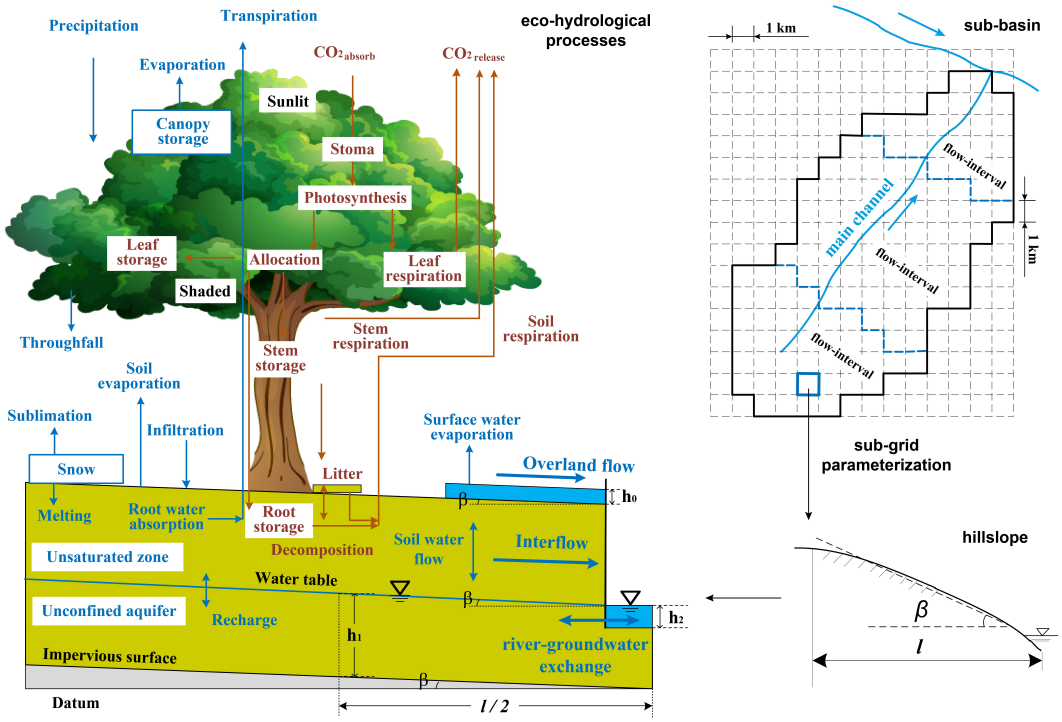

698

699 **Figure 2.** Structure and main eco-hydrological processes for the land surface

700 hydrological model CLM-GBHM. (modified from Jiao et al., 2017)

701

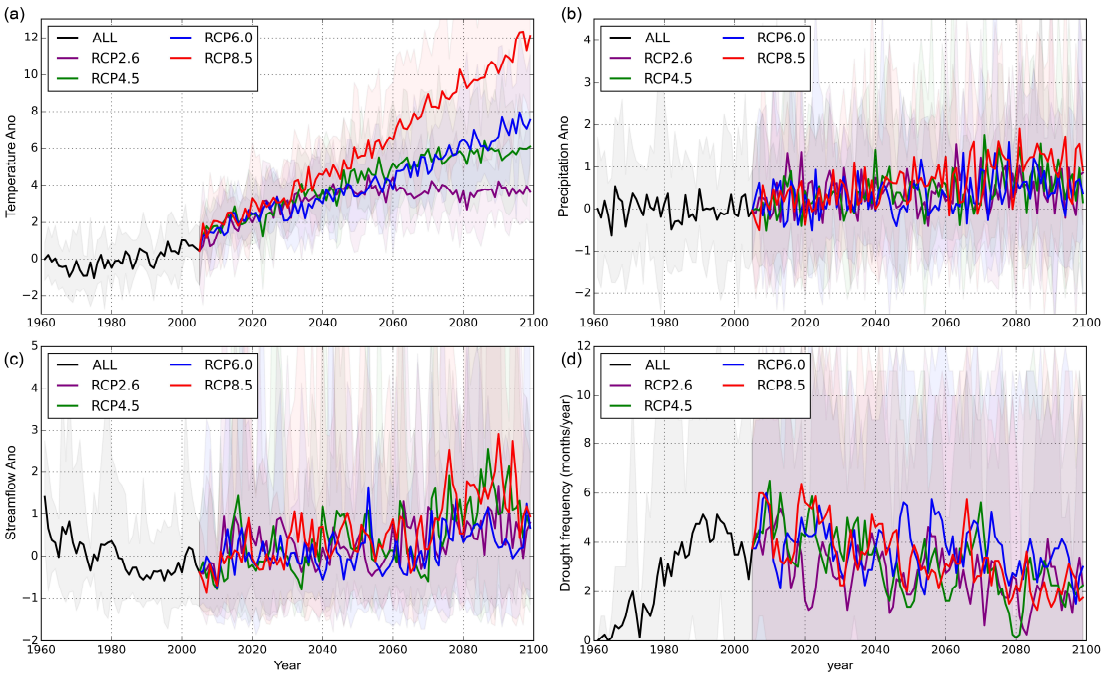

Figure 3. Historical (ALL) and future (RCP2.6/4.5/6.0/8.5) time series of standardized annual mean (a) temperature, (b) precipitation and (c) streamflow, and (d) the time series of hydrological drought frequency (drought months for each year) over the Wudinghe watershed. Shaded areas indicate the ranges between maximum and minimum values among CMIP5/CLM-GBHM model simulations. ALL represents historical simulations with both anthropogenic and natural forcings, RCP2.6/4.5/6.0/8.5 represent four representative concentration pathways from lower to higher emission scenarios.

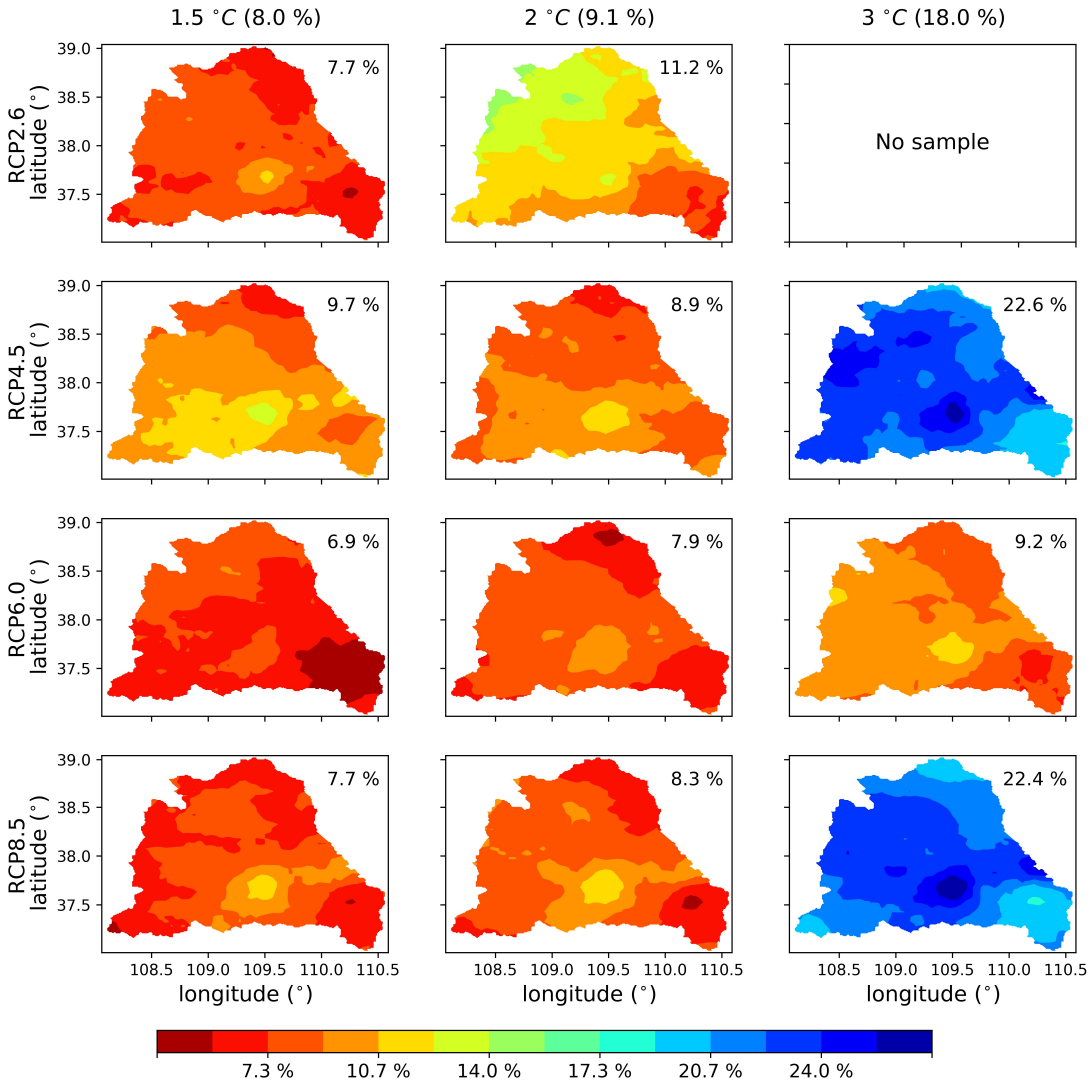

Figure 4. Spatial pattern of relative changes in multi-model ensemble mean precipitation at 1.5, 2 and 3 ℃ warming levels compared to the baseline period (1986-2005). The percentages in the upper-right corners of each panel are the watershed-mean changes for different RCP scenarios, and the percentages in the top brackets are the mean values from four RCP scenarios.

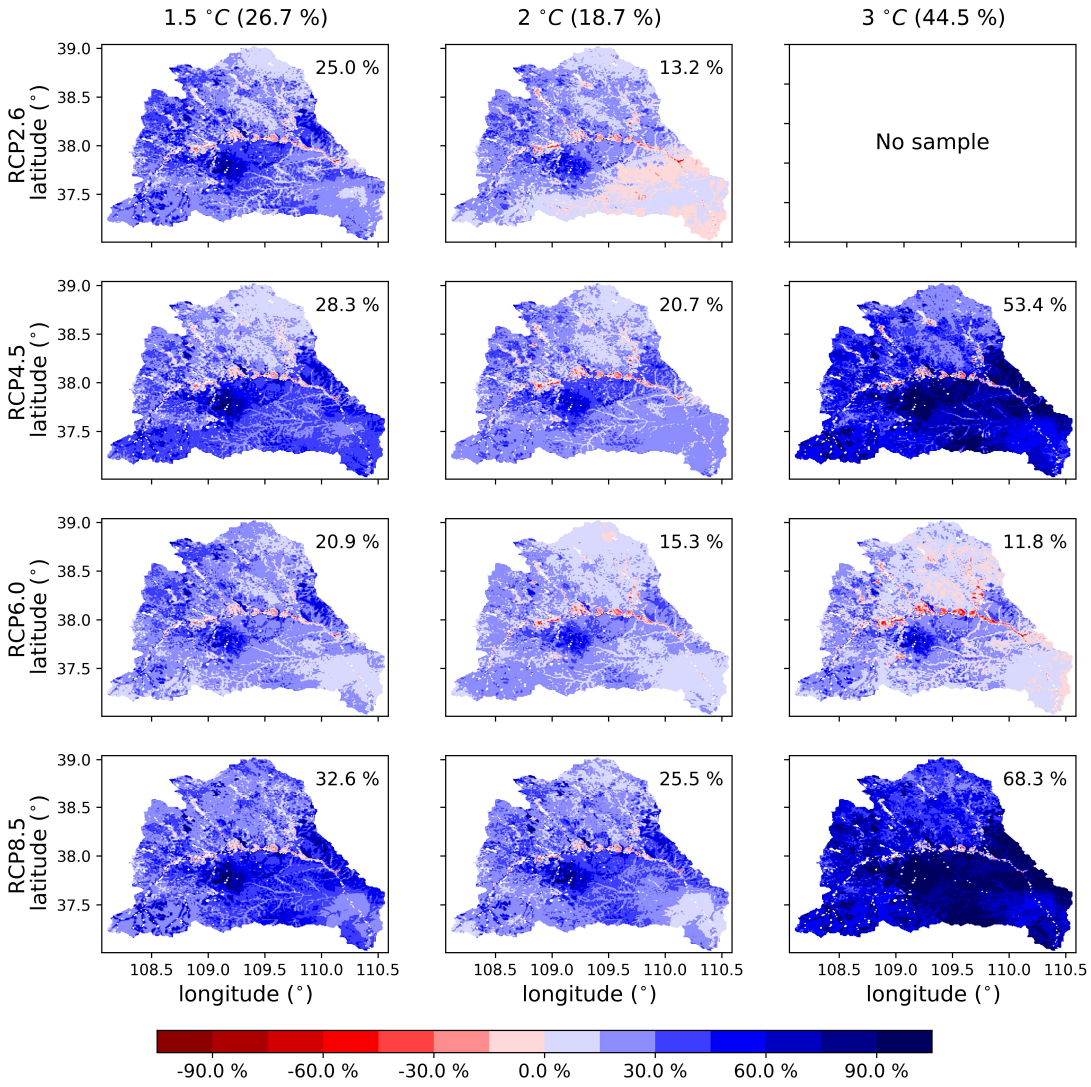

717

718 **Figure 5.** The same as **Figure 4**, but for the spatial patterns of runoff changes.

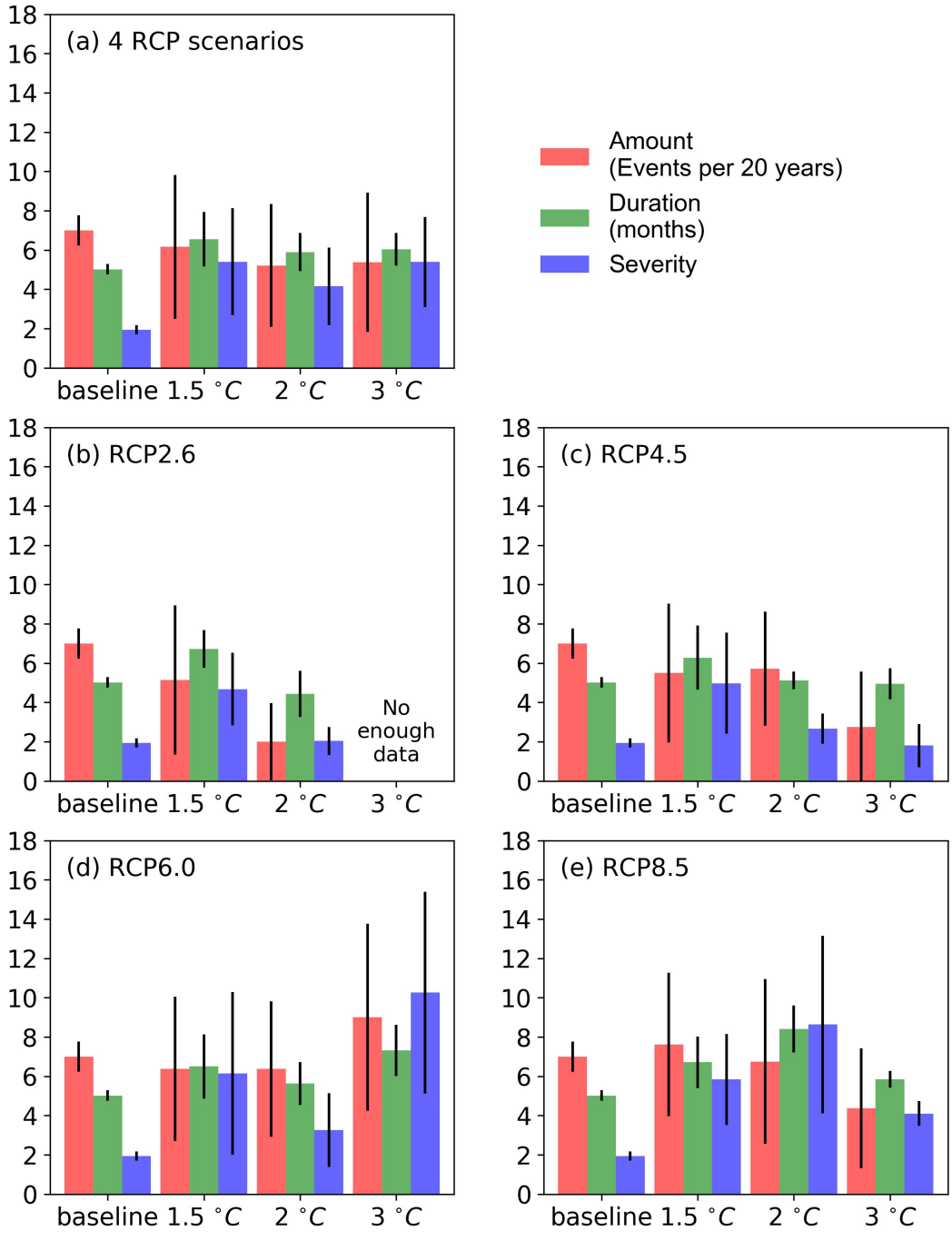

719

720 **Figure 6.** Comparison of the characteristics (amount (number of drought events per
721 20 years), duration (months) and severity) averaged among climate models and RCP
722 scenarios for hydrological drought events during the baseline period (1986-2005) and
723 the periods reaching 1.5, 2 and 3 ℃ warming levels. Black lines indicate 5%-95%
724 confidence intervals.

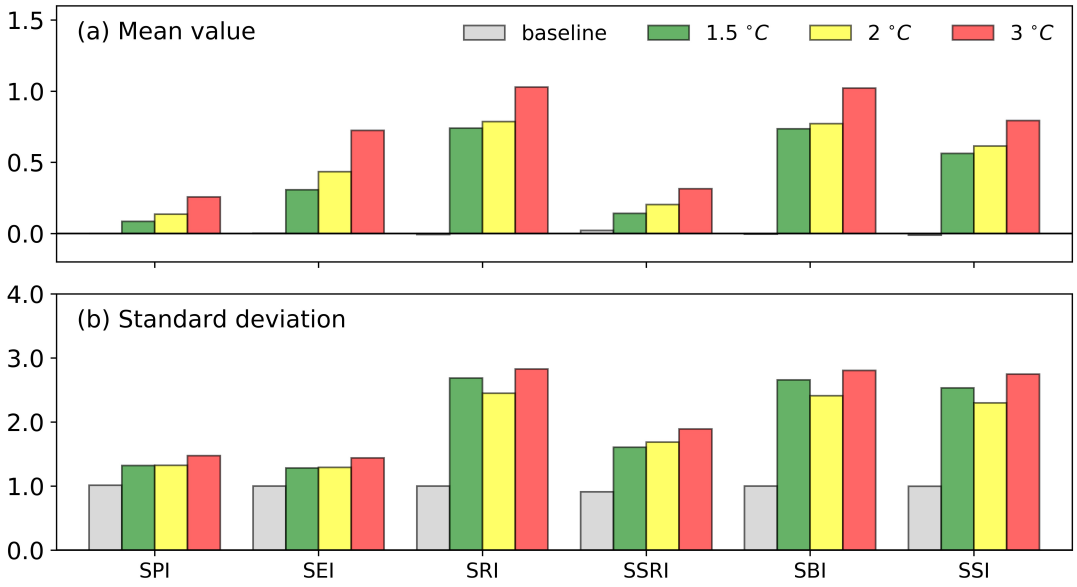

725

726 **Figure 7.** Comparison of (a) mean values and (b) standard deviations for hydrological

727 indices averaged among climate models and RCP scenarios during the baseline period

728 (1986-2005) and the periods reaching 1.5, 2 and 3 ℃ warming levels. SPI, SEI, SRI,

729 SSRI, SBI, SSI represent standardized indices of precipitation, evapotranspiration,

730 runoff, surface runoff, baseflow (subsurface runoff) and streamflow, respectively.

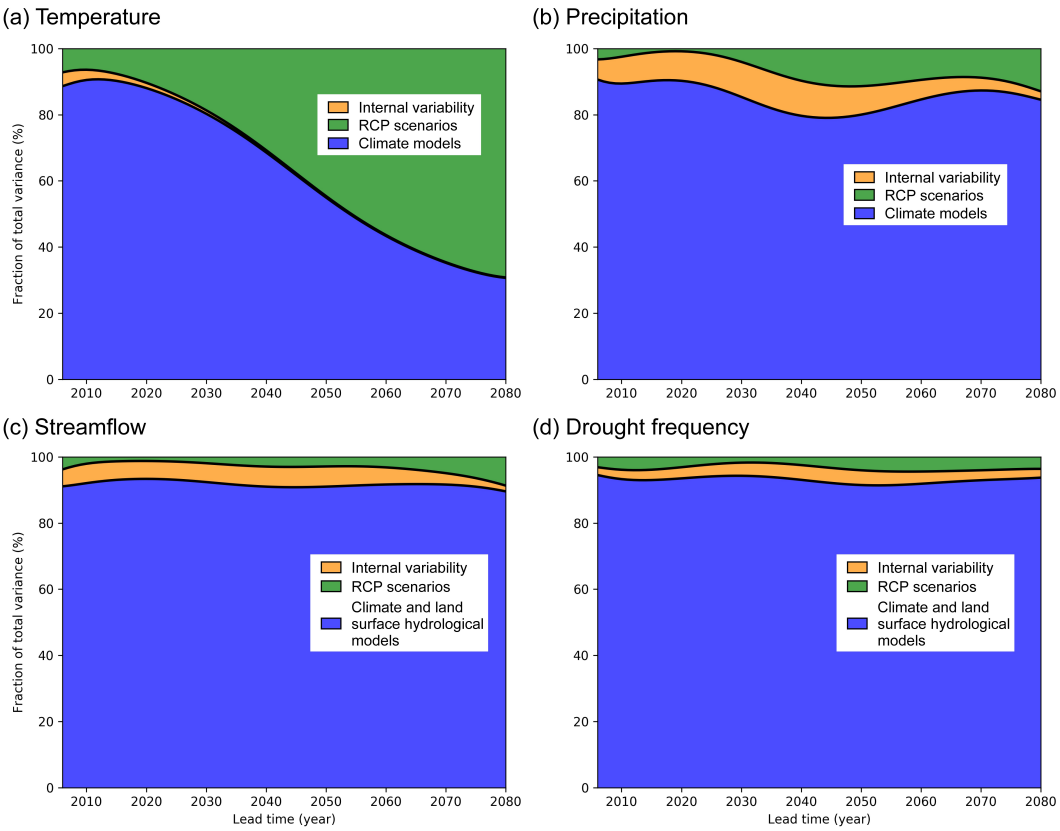

731

732 **Figure 8.** Fractions of uncertainties from internal variability (orange), RCP scenarios

733 (green) and climate and land surface hydrological models (blue) for the projections of

734 20-years moving averaged (a) temperature, (b) precipitation (c) streamflow and (d)

735 hydrological drought frequency.

Table 1. CMIP5 model simulations used in this study. ALL represents historical simulations with both anthropogenic and natural forcings (r1i1p1 realization), RCP2.6/4.5/6.0/8.5 represent four representative concentration pathways from lower to higher emission scenarios.

GCMs	Institute	Resolution	Historical simulations	RCP scenarios
GFDL-CM3	NOAA GFDL	144×90	ALL	RCP2.6/4.5/6.0/8.5
GFDL-ESM2M	NOAA GFDL	144×90	ALL	RCP2.6/4.5/6.0/8.5
HadGEM2-ES	MOHC	192×145	ALL	RCP2.6/4.5/6.0/8.5
IPSL-CM5A-LR	IPSL	96×96	ALL	RCP2.6/4.5/6.0/8.5
IPSL-CM5A-MR	IPSL	144×143	ALL	RCP2.6/4.5/6.0/8.5
MIROC-ESM-CHEM	MIROC	128×64	ALL	RCP2.6/4.5/6.0/8.5
MIROC-ESM	MIROC	128×64	ALL	RCP2.6/4.5/6.0/8.5
MRI-CGCM3	MRI	320×160	ALL	RCP2.6/4.5/6.0/8.5

738 **Table 2.** Trends in hydrometeorological variables and hydrological drought frequency over the Wudinghe watershed. Historical observed trends
739 for streamflow and drought frequency were calculated by using naturalized streamflow data (Yuan et al., 2017). Here, "*" and "**" indicate 90%
740 and 99% confidence levels, respectively, while those without any "*" show no significant changes (p>0.1).

Historical (1961-2005) and future (2006-2099) scenarios	**Changing trend of standardized timeseries (yr^{-1})**			
	Temperature	**Precipitation**	**Streamflow**	**Drought frequency**
(historical) observations	0.0494**	-0.0216*	-0.0503**	0.0448**
(historical) all forcings simulations	0.0272**	-0.0009	-0.0213**	0.0346**
(future) RCP2.6 simulations	0.0138**	0.0025*	0.0046**	-0.0069**
(future) RCP4.5 simulations	0.0291**	0.0056**	0.0105**	-0.0096**
(future) RCP6.0 simulations	0.0312**	0.0039**	0.0038**	-0.0044**
(future) RCP8.5 simulations	0.0345**	0.0108**	0.0133**	-0.0107**

741 **Table 3.** Determination of crossing year for the periods reaching 1.5, 2 and 3 ℃ warming levels for different GCMs and RCPs combinations.

742 Here, "NR" means that the corresponding GCM/RCP combination will not reach the specified warming level throughout the 21st century.

GCMs	1.5 ℃ warming level				2 ℃ warming level				3 ℃ warming level			
	RCP2.6	RCP4.5	RCP6.0	RCP8.5	RCP2.6	RCP4.5	RCP6.0	RCP8.5	RCP2.6	RCP4.5	RCP6.0	RCP8.5
GFDL-CM3	2016	2018	2019	2018	2039	2032	2039	2030	NR	2066	2070	2052
GFDL-ESM2M	NR	2051	2059	2038	NR	NR	2076	2054	NR	NR	NR	2084
HadGEM2-ES	2020	2023	2023	2018	2042	2039	2042	2032	NR	2071	2070	2052
IPSL-CM5A-LR	2030	2029	2031	2025	NR	2045	2049	2037	NR	NR	2086	2057
IPSL-CM5A-MR	2032	2025	2031	2024	NR	2045	2050	2037	NR	NR	2081	2055
MIROC-ESM-CHEM	2019	2024	2026	2020	2037	2038	2042	2032	NR	2075	2070	2051
MIROC-ESM	2026	2025	2032	2024	2048	2039	2046	2033	NR	2080	2076	2056
MRI-CGCM3	2075	2043	2053	2036	NR	2074	2070	2049	NR	NR	NR	2072
Model ensemble	2026	2025	2031	2024	2041	2039	2048	2035	NR	2073	2073	2056
Total ensemble	2025 (2016~2075)				2042 (2030~2076)				2070 (2051~2086)			

743